Proceedings of the 17th World Congress
The International Federation of Automatic Control
Seoul, Korea, July 6-11, 2008

Inverse Optimal Velocity Field Control of an Outdoor Blimp Robot

– Blimp Surveillance Systems for Rescue –

T. Fukao * **A. Yuzuriha** * **T. Suzuki** * **T. Kanzawa** * **T. Oshibuchi** * **K. Osuka** *
T. Kohno ** **M. Okuyama** ** **Y. Tomoi** ** **M. Nakadate** **

* *Department of Mechanical Engineering, Kobe University*
** *Aviation Program Group, Japan Aerospace Exploration Agency*

Abstract: A surveillance system is required to gather the suffering information in the stricken area safely and quickly after natural disasters. An autonomous blimp is the best option for this purpose. Inverse optimal velocity field control is proposed for the blimp to keep a desired trajectory. The desired trajectory based on velocity field is designed, and inverse optimal tracking control is applied to be robust to input uncertainties. The transient performance to the desired trajectory is very important to fly smoothly along the contour, because the blimp is affected by wind easily. The inverse optimal control is expected to improve the robustness to uncertainties of various dynamic parameters. Some experiments are performed to confirm the usefulness of the proposed method by using an outdoor blimp whose length is 12.2m.

1. INTRODUCTION

After natural disasters such as earthquake, tsunami, and flood, a surveillance system is required to gather the suffering information in the stricken area safely and quickly. From the reports of Kobe earthquake, which is called as Great Hanshin-Awaji Earthquake and occurred around Kobe City in Japan in 1995, 72 hours are very important for victims to survive. If 72 hours have passed, the possibility to survive is decreasing largely even if they are rescued. Ground vehicles are hard to carry out the task of searching, because the fallen constructions in urban areas and the fallen trees and landslides in local areas are obstructive to search for survivors especially after earthquakes.

Aerial vehicles are the candidate of collecting information. Unmanned aerial vehicles (UAVs) are better options to perform the task precisely, safely, and quickly. Especially an autonomous blimp is the best option. It is a kind of LTA (Lighter Than Air) vehicles and it has some advantages beyond the other UAVs like helicopters or planes with regard to safety for victims, easy use to fly, high mileage, and lower-sky availability. The blimp flying in low sky can capture good quality images to offer 3D images in disasters. The integration and representation of the suffering information in the stricken area are required for rapid rescue planning before rescue activities. For this purpose, we propose the autonomous blimp system shown in Fig. 1 with the rotational stereo camera system designed like Fig. 2. This camera system is very useful to get much information of three dimensional buildings and houses because the rotational motion as flying permits to get occluded points and surfaces.

The blimp is naturally designed as an underactuated system, that is, there is no actuator to move directly in the lateral direction, because the loss of energy is large. We have to consider the effect of wind and design a robust control system for the blimp. In this paper, we propose in-

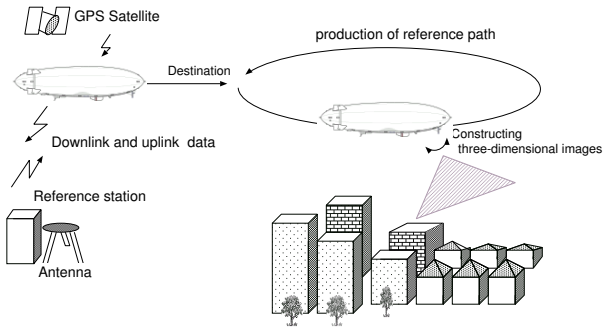

Fig. 1. Illustration of the proposed system

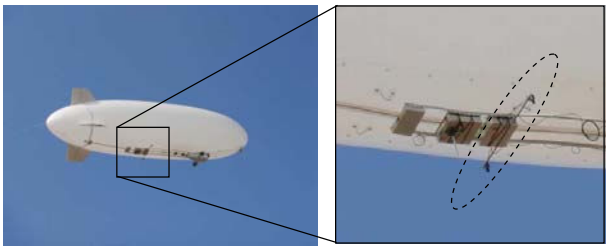

Fig. 2. Rotational stereo camera

verse optimal velocity field control of an outdoor blimp. A desired trajectory based on velocity field [Li and Horowitz, 2003, Dixon et al., 2005] is designed, and inverse optimal tracking control [R. Sepulchre and Kokotovic, 1996, Fukao, 2004] is applied to be robust with input uncertainties. The velocity field is time invariant and consists of the desired contours which are provided by velocity tangent vectors. This is highly meaningful for the blimp which is affected by wind easily, because the transient performance to the desired trajectory is important to fly smoothly along the contour. The inverse optimal control is extremely useful to improve the robustness to input uncertainties which include slowly varying dynamic parameters. The robustness was

proved for nonholonomic wheeled mobile robots [Fukao, 2004]. One of alternatives is adaptive control for underactuated systems with dynamic uncertainties [Dixon et al., 2005, Fukao et al., 2000], but it is very hard to adjust many gains of adaptive updating rules and control gains through our experiments of indoor blimp [Fukao et al., 2003a,b]. We perform some experiments to confirm the usefulness of the proposed method by using an outdoor blimp whose length is 12.2m (40feet).

2. DESIGN OF A CONTROL SYSTEM FOR A BLIMP

We show how to set a desired trajectory based on velocity field and design an inverse optimal tracking controller which is robust to input uncertainties. This approach is confirmed to be appropriate for a blimp which is affected by wind.

2.1 Velocity field

On usual tracking control problems, the task of a robot is to track a prespecified trajectory which depends on time, that is, the control objective is to reduce the tracking error as time passes. But this type of tracking control is not sufficient for contour following whose objective is to reduce the contouring error. The relationship is shown in Fig. 3 [Li and Horowitz, 2003].

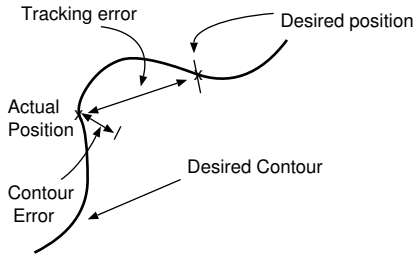

Fig. 3. Tracking error and contouring error

From this point of view, velocity field control has proposed [Li and Horowitz, 2003]. The velocity field is time invariant and consists of the desired contours which are provided by velocity tangent vectors. In Fig. 4, a circular contour is encoded by a velocity field. The velocity field control approach intends to avoid the timing issue in a timed trajectory formation which is restrictive for contour following tasks.

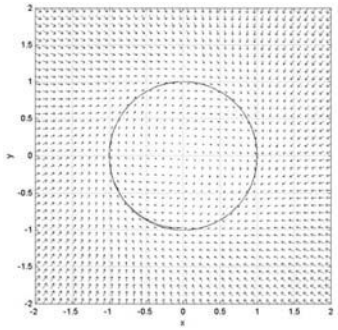

Fig. 4. Circular velocity field

In addition, from the different point of view, we expect velocity field control works for a blimp. A blimp should be flying almost parallel to the wind direction because it is affected by wind easily and a gust from the side makes the blimp slide largely. This means the transient performance to the desired trajectory is so important that the smooth movement along a contour with a velocity tangent vector is expected to avoid undesirable behaviors. One example of reference trajectory is shown in Fig. 5.

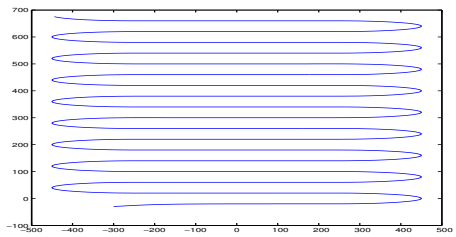

Fig. 5. One example of reference trajectory

2.2 Kinematic controller

In the same way of the indoor blimp, the vertical motion is assumed to be compensated by a separate simple controller [Fukao et al., 2003a,b], which is described later. We consider the two dimensional motion shown in Fig. 6, where $O - xy$ is a two dimensional coordinate system.

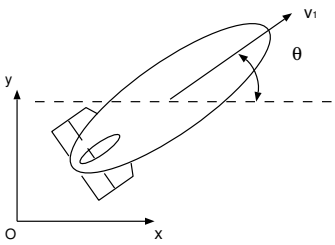

Fig. 6. Kinematic model of a blimp on a plane

We set the generalized coordinates as following:

$$q = [\, x_c \;\; y_c \;\; \theta \,]^T, \tag{1}$$

where x_c, y_c, $\theta(t) \in$R represent the position of the center of gravity and the direction of the body axis.

We assume the following conditions [Fukao et al., 2003a,b].

Assumption 2.1. The rolling motion and pitching motion are neglected. The center of gravity and the center of buoyancy are on the vertical axis of a blimp. The axis on yawing motion is the same vertical one. □

The kinematics of a blimp is provided as following:

$$\dot{q} = S(q)v, \tag{2}$$

where $v(t) = [\, v_1 \;\; v_2 \,]^T \in R^2$ with the transitional velocity v_1 and the yaw rate v_2 of the center of gravity, and the matrix $S(q)$ is defined as

$$S(q) = \begin{bmatrix} \cos\theta & 0 \\ \sin\theta & 0 \\ 0 & 1 \end{bmatrix}. \tag{3}$$

2.3 Design of velocity field

A design method of velocity field for a wheeled mobile robot was proposed in Dixon et al. [2005]. We refer to the method for a blimp because the kinematics of a blimp except the vertical motion is assumed to be same as a wheeled mobile robot as described above.

The desired velocity field is defined as following:

$$\vartheta(q) = \begin{bmatrix} \dot{x}_d \\ \dot{y}_d \\ \dot{\theta}_d \end{bmatrix} = \begin{bmatrix} \cos\theta_d(q) & 0 \\ \sin\theta_d(q) & 0 \\ 0 & 1 \end{bmatrix} v_d(q), \tag{4}$$

where $v_d(q) = [\, v_{d1} \;\; v_{d2} \,]^T \in R^2$, and $\vartheta(q)$, $\dot{x}_d$, $\dot{y}_d$, $\frac{\partial\, \vartheta(q)}{\partial\, q}$ are designed to be bounded. The velocity field is also designed such that $\lim_{t\to\infty} ||v_d(t)|| \neq 0$.

Circular velocity field

For a desired contour of a circle around the origin with a radius of R, the velocity field is derived by referring to Dixon et al. [2005]. In the desired velocity field (4), θ_d is given by

$$\theta_d(q) = \arctan 2\ (\rho_2(q),\ \rho_1(q)), \tag{5}$$

where arctan2$(\cdot)$ is the four quadrant inverse tangent function, $\pi < \theta_d \leq \pi$, and

$$v_{1d} = \sqrt{\rho_1^2(q) + \rho_2^2(q)}, \tag{6}$$

$$v_{2d} = \dot{\theta}_d \tag{7}$$

$$= \begin{cases} \dfrac{d}{dt}\ \arctan 2\ (\rho_2(q),\ \rho_1(q)), & -\pi < \theta_d < \pi \\ 1, & \theta_d = \pi \end{cases}$$

with the auxiliary functions ρ_1, $\rho_2 \in$ R are defined as

$$\rho_1(q) = k_1(R^2 - x_c^2 - y_c^2)x_c + k_2 y_c, \tag{8}$$

$$\rho_2(q) = k_1(R^2 - x_c^2 - y_c^2)y_c - k_2 x_c, \tag{9}$$

where k_1 and k_2 are added to adjust the desired velocity.

In (7), $\dot{\theta}_d$ is rewritten as

$$\dot{\theta}_d = \begin{bmatrix} \dfrac{\partial\theta_d}{\partial x_c} & \dfrac{\partial\theta_d}{\partial y_c} \end{bmatrix} \begin{bmatrix} \dot{x_c} \\ \dot{y_c} \end{bmatrix}, \tag{10}$$

where

$$\frac{\partial\theta_d}{\partial x_c} = \begin{bmatrix} \dfrac{-\rho_2}{\rho_1^2+\rho_2^2} & \dfrac{\rho_1}{\rho_1^2+\rho_2^2} \end{bmatrix} \begin{bmatrix} \dfrac{\partial\rho_1}{\partial x_c} \\ \dfrac{\partial\rho_2}{\partial x_c} \end{bmatrix}, \tag{11}$$

$$\frac{\partial\theta_d}{\partial y_c} = \begin{bmatrix} \dfrac{-\rho_2}{\rho_1^2+\rho_2^2} & \dfrac{\rho_1}{\rho_1^2+\rho_2^2} \end{bmatrix} \begin{bmatrix} \dfrac{\partial\rho_1}{\partial y_c} \\ \dfrac{\partial\rho_2}{\partial y_c} \end{bmatrix}. \tag{12}$$

Then, the following equation is derived from (8) – (12)

$$\dot{\theta}_d = \begin{bmatrix} \dfrac{-\rho_2}{\rho_1^2+\rho_2^2} & \dfrac{\rho_1}{\rho_1^2+\rho_2^2} \end{bmatrix} \begin{bmatrix} \dfrac{\partial\rho_1}{\partial x_c} & \dfrac{\partial\rho_1}{\partial y_c} \\ \dfrac{\partial\rho_2}{\partial x_c} & \dfrac{\partial\rho_2}{\partial y_c} \end{bmatrix}$$

$$\begin{bmatrix} k_1(R^2 - x_c^2 - y_c^2)x_c + k_2 y_c \\ k_1(R^2 - x_c^2 - y_c^2)y_c - k_2 x_c \end{bmatrix}. \tag{13}$$

Fig. 4 shows the case of $R = 1.0$ and $k_1 = k_2 = 1$.

Straight velocity field

For a desired contour of a straight line, a desired velocity field (4) is designed. The auxiliary functions ρ_1, ρ_2 of $\theta_d(q)$ are provided by

$$\rho_1(q) = k_v, \tag{14}$$

$$\rho_2(q) = -c_2 y_c, \tag{15}$$

where k_v is the constant velocity along x axis and c_2 is the rate of convergence to y axis. $\dot{\theta}_d$ is calculated as

$$\dot{\theta}_d = \begin{bmatrix} \dfrac{-\rho_2}{\rho_1^2+\rho_2^2} & \dfrac{\rho_1}{\rho_1^2+\rho_2^2} \end{bmatrix} \begin{bmatrix} \dfrac{\partial\rho_1}{\partial x_c} & \dfrac{\partial\rho_1}{\partial y_c} \\ \dfrac{\partial\rho_2}{\partial x_c} & \dfrac{\partial\rho_2}{\partial y_c} \end{bmatrix} \begin{bmatrix} k_v \\ -c_2 y_c \end{bmatrix}.$$

One example is shown in Fig. 7 in the case of $c_2 = 3.0$, $k_v = 10.0$.

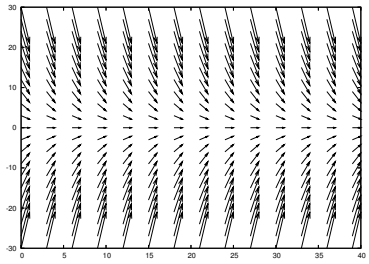

Fig. 7. Straight velocity field

2.4 Kinematic control

As a kinematic controller of a blimp, we apply an inverse optimal control approach [R. Sepulchre and Kokotovic, 1996] which we introduced to nonholonomic mobile robots and showed the robustness [Fukao, 2004]. This was also shown to be very useful for image-based control of an indoor blimp [Fukao et al., 2005].

Inverse optimal design

The optimal stabilizing control problem [Sepulchre et al., 1991] is to find a feedback control $u(x)$ for the system

$$\dot{x} = f(x) + g(x)u, \tag{16}$$

with the following properties:

(1) $u(x)$ achieves asymptotic stability of the equilibrium $x = 0$.
(2) $u(x)$ minimizes the cost functional

$$J = \int_0^\infty (l(x) + u^T R(x) u)dt \tag{17}$$

where $l(x)$ is positive semidefinite and $R(x)$ is positive definite matrix for all x.

We have to solve the following Hamilton-Jacobi-Bellman equation

$$l(x) + L_f V(x) - \frac{1}{4} L_g V(x) R^{-1}(x) (L_g V(x))^T = 0, \quad V(0) = 0, \tag{18}$$

where $V(x)$ is a positive semidefinite scalar function and $L_f V(x)$ is a Lie derivative which is defined as $\frac{\partial f}{\partial x} V(x)$. But this task is not feasible in general.

We consider the inverse approach where a stabilizing feedback is designed first and shown to be optimal for a cost functional as (17) [Li and Slotine, 1997]. The following concept of a control Lyapunov function (CLF) of Artstein [Arstein, 1983] and Sontag [Sontag, 1983] plays an important role for the approach.

Definition 2.1. (Control Lyapunov function)
A smooth, positive definite, and radially unbounded function $V(x)$ is called a control Lyapunov function (CLF) for the system (16) if for all $x \neq 0$,

$$L_g V(x) = 0 \quad \Rightarrow \quad L_f V(x) < 0. \tag{19}$$

□

Proposition 2.1. (Optimal stabilizing control from a CLF)
The control law given by Sontag's formula:

$$u(x) = \begin{cases} -\left(c_0 + \dfrac{a(x) + \sqrt{a^2(x) + (b^T(x)b(x))^2}}{b^T(x)b(x)} \right) b(x), & b(x) \neq 0 \\ 0, & b(x) = 0 \end{cases} \tag{20}$$

is optimal stabilizing for the cost functional

$$J = \int_0^\infty \left(\frac{1}{2} p(x) b^T(x) b(x) + \frac{1}{2p(x)} u^T u \right) dt \tag{21}$$

where $a(x)$, $b(x)$, $p(x)$ are defined by

$$a(x) = L_f V(x), \tag{22}$$

$$b(x) = L_g V(x), \tag{23}$$

$$p(x) = \begin{cases} c_0 + \dfrac{a(x) + \sqrt{a^2(x) + (b^T(x)b(x))^2}}{b^T(x)b(x)}, & b(x) \neq 0 \\ c_0, & b(x) = 0 \end{cases} \tag{24}$$

with a CLF $V(x)$. □

A consequence of the optimality is that the designed system by the control law (20) has a stability margin called sector margin $(\frac{1}{2}, \infty)$. The sector margin is defined as the following definition [Sepulchre et al., 1991].

Definition 2.2. (Sector margin)
The nonlinear feedback system (H, k), which consists of a nonlinear plant H and a control law k, shown in Fig. 8 is said to have a sector margin (α, β) if the perturbed closed-loop system (H, k, Δ) is globally asymptotically stable for any input uncertainty Δ which is of the form diag$\{ \psi_1(\cdot), \ldots, \psi_m(\cdot) \}$ where $\psi_i(\cdot)$s are locally Lipschitz static nonlinearities which belong to the sector (α, β). □

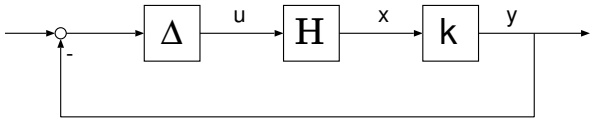

Fig. 8. Nonlinear feedback loop with control $k(x)$ and uncertainty Δ

We apply this inverse optimal tracking control design to an underactuated outdoor blimp robot in the following.

Inverse optimal tracking control of a blimp

For a kinematic model, we define the error coordinates:

$$\begin{bmatrix} x_e \\ y_e \\ \theta_e \end{bmatrix} = \begin{bmatrix} \cos\theta & \sin\theta & 0 \\ -\sin\theta & \cos\theta & 0 \\ 0 & 0 & 1 \end{bmatrix} \begin{bmatrix} x_d - x_c \\ y_d - y_c \\ \theta_d - \theta \end{bmatrix}, \tag{25}$$

where x_e, y_e, θ_e are the relative errors between a real robot and a reference robot.

The error equation is derived as

$$\begin{aligned} \dot{x}_e &= v_2 y_e - v_1 + v_{d1} \cos\theta_e, \\ \dot{y}_e &= -v_2 x_e + v_{d1} \sin\theta_e, \\ \dot{\theta}_e &= v_{d2} - v_2. \end{aligned} \tag{26}$$

To design an inverse optimal tracking controller, we select a CLF referring the Lyapunov function provided in Jiang and Nijmeijer [1997] which is designed for the semi-global tracking controller.

First, we define a function:

$$\varphi(s) = \frac{s}{1 + s^2}, \tag{27}$$

which satisfies the conditions that $s\varphi(s) > 0$, $\forall s \neq 0$, and $\varphi(0) = 0$.

Then, we transform the coordinate as

$$\bar{\theta}_e = \theta_e + \varphi(y_e v_{d1}). \tag{28}$$

The error equation (26) is represented as

$$\begin{aligned} \dot{x}_e &= v_2 y_e - v_1 + v_{d1} \cos(\bar{\theta}_e - \varphi), \\ \dot{y}_e &= -v_2 x_e + v_{d1} \sin(\bar{\theta}_e - \varphi), \\ \dot{\bar{\theta}}_e &= v_{d2} - v_2 \\ &\quad + \varphi'(-v_2 x_e v_{d1} + v_{d1}^2 \sin(\bar{\theta}_e - \varphi) + y_e \dot{v}_{d1}), \end{aligned} \tag{29}$$

where $\varphi'(s)$ means the derivative of $\varphi(s)$ at s, that is, $\varphi'(s) = \frac{1 - s^2}{(1 + s^2)^2}$.

We rewrite the error equation (29) as the normal form of nonlinear systems like the system (16):

$$\frac{\mathrm{d}}{\mathrm{dt}} \begin{bmatrix} x_e \\ y_e \\ \bar{\theta}_e \end{bmatrix} = \begin{bmatrix} v_{d1} \cos(\bar{\theta}_e - \varphi) \\ v_{d1} \sin(\bar{\theta}_e - \varphi) \\ v_{d2} + \varphi'(v_{d1}^2 \sin(\bar{\theta}_e - \varphi) + y_e \dot{v}_{d1}) \end{bmatrix} + \begin{bmatrix} -1 & y_e \\ 0 & -x_e \\ 0 & -1 - \varphi' x_e v_{d1} \end{bmatrix} \begin{bmatrix} v_1 \\ v_2 \end{bmatrix}$$

$$\equiv f + [\, g_1 \;\; g_2 \,] \begin{bmatrix} v_1 \\ v_2 \end{bmatrix}. \tag{30}$$

The following function satisfies the condition (19) as a CLF [Fukao, 2004], and the controller (20) is designable:

$$V(x_e, y_e, \bar{\theta}_e) = \frac{1}{2}k_1 x_e^2 + \frac{1}{2}k_2 y_e^2 + \frac{1}{2}k_3 \bar{\theta}_e^2, \tag{31}$$

where k_1, k_2, k_3 are positive constants, and

$$L_{g_1} V = -k_1 x_e, \tag{32}$$

$$L_{g_2} V = (k_1 - k_2) x_e y_e - k_3 \bar{\theta}_e (1 + \varphi' x_e v_{d1}), \tag{33}$$

$$\begin{aligned} L_f V = {} & k_1 x_e v_{d1} \cos(\bar{\theta}_e - \varphi) + k_2 y_e v_{d1} \sin(\bar{\theta}_e - \varphi) \\ & + k_3 \bar{\theta}_e \{ v_{d2} + \varphi' (v_{d1}^2 \sin(\bar{\theta}_e - \varphi) + y_e \dot{v}_{d1}) \}. \end{aligned} \tag{34}$$

Remark 2.1. As examples of the uncertainties, the relationship between the velocity of the outdoor blimp and the power of two engines cannot be measured correctly, and the dynamic parameters of the blimp are variable according to the altitude and temperature. Consequently, the inverse optimal approach is expected to be effective to such a blimp with input uncertainties [Fukao, 2004].

3. SIMULATION

3.1 Velocity field of a desired trajectory

The velocity field of the desired trajectory to capture images by a rotational stereo camera consists of long lines and turning half circles shown in Fig. 5 because the blimp should fly parallel to the wind not to be affected largely.

The core of the reference trajectory is lines and half circles. Therefore, we consider the simplified trajectory shown in Fig. 9. This is designed by setting appropriate functions ρ_1, ρ_2, and $\dot{\theta}_d$, although the continuity is not completed.

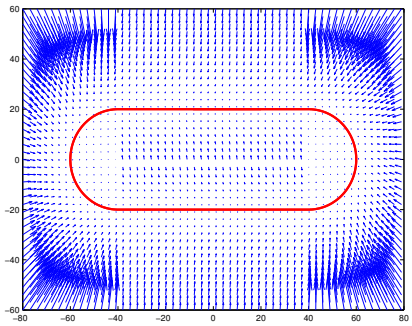

Fig. 9. Velocity field of reference path for simulation

3.2 Simulation results

We perform a simulation in the case of no wind by the above method, where the velocity field is like Fig. 9. The initial configuration is $x = -40$, $y = 20$ and $\theta = 0$. The radius of half circle is $R = 20$, and the parameters of velocity field are $k_v = 20.0$, $c_1 = 400.0$. The length of straight line is $w = 40$, and the parameter of velocity field is $c_2 = 1.0$. The control gains are $c_0 = 0.1$, $k_1 = 100.0$, $k_2 = 100.0$, $k_3 = 1.0$. The simulation result is shown in Fig. 10.

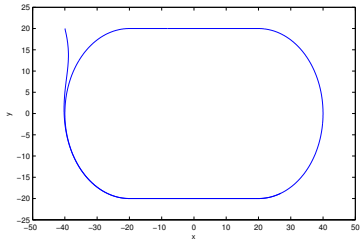

Fig. 10. Simulation result

4. OUTDOOR EXPERIMENT

4.1 Configuration of the blimp

Our blimp is shown in Fig. 11.

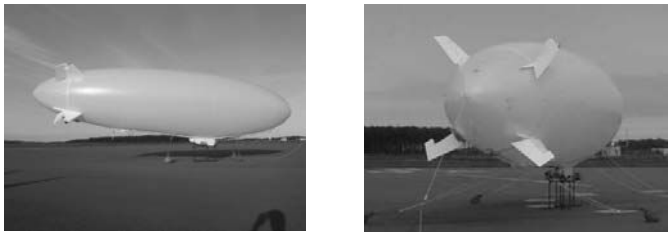

Fig. 11. Pictures of the blimp

Its length is about 12.2m (40feet). It has two 62cc engines and a X tail wing system. It also has a thruster and a baronet system. The payload is about 15kg which depends on temperature. The loaded equipments are a small PC with WLAN, a RTK-GPS, an IMU, a wind sensor, and a rotational stereo camera. The outline is also shown in Fig. 12.

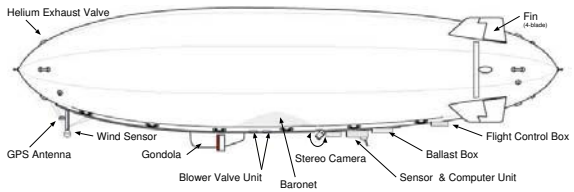

Fig. 12. Outline of the blimp

The system architecture is also drawn in Fig. 13.

4.2 Experimental results

We performed many experiments. One example is shown in Fig. 14. The desired trajectory is a straight line whose length 30m, a left turn whose radius is 15m, and a straight line. The results are shown in Fig. 14. The origin of the position is the position when starting to control. The average wind speed is about 3m/s.

We cannot control the velocities directly and have to compensate the error between the kinematic control v_1 and v_2 provided by (20) and the real velocities.

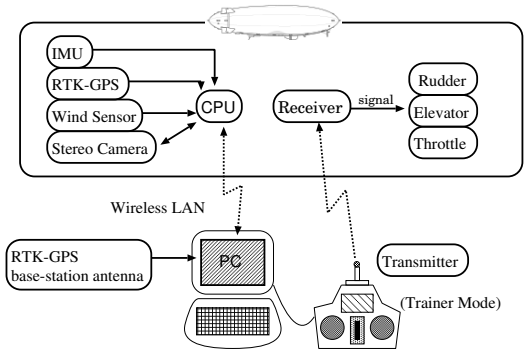

Fig. 13. System architecture

The real control input is given by the followings:

$$\tau_1 = K_{d1}(\acute{v_1} - v_1), \tag{35}$$

$$\tau_2 = K_{d2}(\acute{v_2} - v_2), \tag{36}$$

where $\acute{v_1}$, $\acute{v_2}$ are the real velocities, and K_{d1}, K_{d2} are positive constants.

Furthermore, the control input to keep the altitude constant is simply provided by

$$\tau_3 = K_{d3}(h - h_d), \tag{37}$$

where h is the real altitude, h_d is the desired, and K_{d3} is positive. The separation from the other motion is assumed and it works under mild wind.

The control parameters are provided in Tab. 1.

Table 1. Control parameters

Velocity Field		Kinematics		Dynamics	
c_1	1400.0	c_0	0.1	K_{d1}	1.0
c_2	1.0	k_1	100.0	K_{d2}	1.0
k_v	3.0	k_2	100.0	K_{d3}	1.0
		k_3	1.0		

From these experiments, the proposed method was confirmed to work well in wind. As a comparison, we applied Kanayama's method [Kanayama et al., 1990] based on velocity field, but it failed completely. Furthermore, the blimp system was confirmed to be a very safe system in low sky. It is very important for a surveillance system in disasters. The remaining issue is that the current system cannot deal with strong wind. It seems that the reason is the neglection of the pitching motion. We are extending the method and developing a new control system.

5. CONCLUSION

An inverse optimal control system for a blimp was proposed to keep a desired trajectory based on velocity field. From the experiments, the proposed method was confirmed to work well in mild wind.

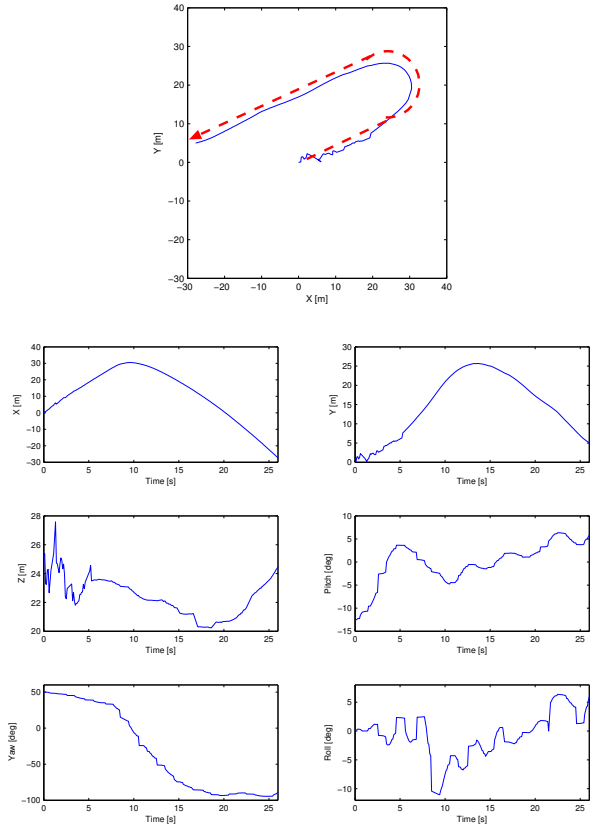

Fig. 14. Experimental results

REFERENCES

Z. Arstein. Stabilization with relaxed controls. *Nonlinear Analysis*, 7:1163–1173, 1983.

W. E. Dixon, T. Galluzo, G. Hu, C. Crane, J. Li, and P. Li. Adaptive velocity field control of a wheeled mobile robot. Technical report, Department of Mechanical and Aerospace Engineering, University of Florida, Gainesville, FL 32611-6250, 2005.

T. Fukao. Inverse optimal tracking control of a nonholonomic mobile robot. In *Proc. IEEE/RSJ International Conference on Intelligent Robots and Systems*, pages 1475–1480, 2004.

T. Fukao, K. Fujitani, and T. Kanade. An autonomous blimp for a surveillance system. In *Proc. IEEE/RSJ Int. Conf. Intelligent Robots and Systems*, pages 1820–1825, 2003a.

T. Fukao, K. Fujitani, and T. Kanade. Image-based tracking control of a blimp. In *Proc. 42th IEEE Conference on Decision and Control*, pages 5414–5419, 2003b.

T. Fukao, T. Kanzawa, and K. Osuka. Inverse optimal tracking control of an aerial blimp robot. In *Proc. of 5th International Workshop on Robot Motion and Control*, 2005.

T. Fukao, H. Nakagawa, and N. Adachi. Adaptive tracking control of a nonholonomic mobile robot. *IEEE Transactions on Robotics and Automation*, 16(5):609–615, 2000.

Z. P. Jiang and H. Nijmeijer. Tracking control of mobile robots: A case study in backstepping. *Automatica*, 33(7):1393–1399, 1997.

Y. Kanayama, Y. Kimura, F. Miyazaki, and T. Noguchi. A stable tracking control method for an autonomous mobile robot. In *Proc. IEEE Int. Conf. on Robotics and Automation*, pages 384–389, 1990.

P. Li and R. Horowitz. Passive velocity field control of mechanical manipulators. *IEEE Trans. on Robotics and Automation*, 15(4): 751–763, 2003.

W. Li and J. Slotine. *Applied Nonlinear Control*. Springer-Verlag, 1997.

M. Jankovic R. Sepulchre and P. Kokotovic. *Constructive Nonlinear Control*, chapter 3. Springer-Verlag, 1996.

R. Sepulchre, M. Jankovic, and P. Kokotovic. *Constructive Nonlinear Control*. Prentice Hall, 1991.

E. D. Sontag. A Lyapunov-like characterization of asymptotic controllability. *SIAM J. on Control and Optimization*, 21:462–471, 1983.